RSC Advances

ROYAL SOCIETY OF CHEMISTRY

www.rsc.org/advances

Activation of persulfate by Co_3O_4 nanoparticles for orange G degradation

Jing Zhang[1,*], Mengyan Chen[1], Liang Zhu[1,*]

1. Key Laboratory of Integrated Regulation and Resource Development on Shallow Lakes of Ministry of Education, College of Environment, Hohai University, Nanjing, 210098, China

Contact information for corresponding author:

Jing Zhang, E-mail: zhang_jing@hhu.edu.cn, telephone: 86-15050556980

Liang Zhu, E-mail: zhulianghhu@163.com

Abstract

Nano-Co_3O_4 was prepared by precipitation method and successfully applied as a heterogeneous catalyst to activate persulfate (PS). The heterogeneous character of PS activation with nano-Co_3O_4 was more pronounced at neutral pH as indicated by the maximum degradation rate of orange G (OG) and the low concentration of dissolved cobalt ions. The increasing dosages of nano-Co_3O_4 and PS, and the higher temperature rapidly promoted the degradation kinetics of OG. The sulfate radicals ($SO_4^{\cdot -}$) and hydroxyl radicals (•OH) were proved to be the primary oxidative species, although the intensity of DMPO-OH signals were much stronger than that of DMPO-SO_4 due to the fast transformation from DMPO-SO_4 to DMPO-OH. The catalyst presented an acceptable stability through using it in five consecutive runs. The degradation pathways of OG in nano-Co_3O_4/PS process were proposed for the first time based on LC-MS analysis. The effects of Cl^-, NO_3^-, HCO_3^-, Co^{2+}, Fe^{2+} and Mn^{2+} ions, which were usually co-existed as water matrix chemicals with azo-dyes, on OG removal by nano-Co_3O_4/PS were examined intensively. The reactivity of potassium persulfate (PS), sodium persulfate (NaPS) and potassium peroxymonosulfate (PMS) in the presence of nano-Co_3O_4 followed the order of nano-Co_3O_4/PMS > nano-Co_3O_4/PS > nano-Co_3O_4/NaPS.

Keywords

Nano-Co_3O_4, Sulfate radical, Hydroxyl radical, Heterogeneous catalysis, Co-existing chemicals

1 Introduction

As one of the advanced oxidation processes (AOPs), sulfate radical based AOPs has become a hotspot and been widely studied for the decomposition of various kinds of recalcitrant or hazardous organic compounds due to its high oxidizing ability. Sulfate radicals can be generated by activation of persulfate (PS) or peroxymonosulfate (PMS) with UV [1], heat [2], sono [3], base [4], granular activated carbon [5], quinones [6], phenols [7], transition metals [8], or magnetic spinel [9, 10]. Among these methods, activation of PS with transition metal ions is commonly used and an efficient method to generate sulfate radicals. Among the transition metal ions (Co^{2+}, Cu^{2+}, Ni^{2+}, Fe^{2+}, Ag^{+}, Ru^{3+}) effective for activating PS or PMS, Co mediated decomposition of persulfate (Co/PS) is an efficient catalytic system that can form $SO4^{\cdot -}$ as the major oxidizing species.[11, 12] The Co/PS system for the degradation of contaminants has shown a lot of interests due to its advantages such as high efficiency at wide pH range, small amounts of cobalt catalyst and high efficiency in both carbonate and phosphate buffer solutions.[11]

Previous studies on Co/PS system mainly focused on homogeneous catalysis, where cobalt ions have to be separated at the end of the treatment by precipitation due to their toxic nature and thus need additional operational costs.[8, 11, 12] To avoid the drawback of the homogeneous Co/PS reagent and broaden the application of the reagent, Dionysiou group investigated heterogeneous activation of PMS with Co_3O_4 and found this system had good performance on degradation of 2,4-dichlorophenol.[13] Recently, the composite oxides of cobalt and another metal element have attracted a

great deal of research interest [14, 15] in order to promote the performance of catalysts, for example the Co-Fe bimetallic oxides ($CoFe_2O_4$) [16] and Co-Mn oxides ($Co_xMn_{3-x}O_4$, x=1, 2) [17]. Nano-scaled catalysts also draw much attention in recent years due to their particular physical and chemical properties, and excellent performance.[18, 19] Hence reducing the diameter of Co_3O_4 to nano-scale may enhance the reactivity. Chen et al. proved that nano-Co_3O_4 was an effective activator for PMS to decompose Acid Orange 7 at both acid and neutral pH conditions.[20] Saputra et al. also reported that nano-Co_3O_4 of 24 nm could fast and completely remove phenol in about 20 min, at the conditions of 25 mg L^{-1} phenol, 0.4 g L^{-1} catalyst, 2 g L^{-1} oxone and 25 ^oC.[21] However, the size effect of Co_3O_4 on the catalytic performance was still unclear. Therefore, in this study both the synthetic nano-Co_3O_4 particles and the commercial Co_3O_4 powder were employed as catalysts to activate PS. It should be noted that most of the studies employed nano-Co_3O_4 as heterogeneous catalyst were performed with PMS as a source of $SO4^{\cdot -}$ rather than PS. Thus in this research, the performance discrepancy of PMS and PS in the presence of nano-Co_3O_4 was compared and discussed.

The degradation of target organics may occur on the catalyst surface (i.e., heterogeneous reaction) and/or in the bulk solution (i.e., homogeneous reaction). The contribution from heterogeneous or homogeneous reaction was still uncovered in the nano-Co_3O_4/PS system. The stability and reusability of the catalyst are critical in catalyzed reactions, especially for practical industrial applications. Tan et al. has reported that in nano-Fe_3O_4/PMS process, the stability of nano-Fe_3O_4 decreased

significantly from the first run to the third run.[22] Chen et al. declared that the stability of nano-Co_3O_4 remained almost unchanged in PMS solution. By analyzing their results, we found the activity of nano-Co_3O_4 decreased steady actually, but the slight decline was covered by the long enough reaction time and all the Acid Orange 7 was decomposed at the end of reaction. Therefore, the stability of nano-Co_3O_4 in consecutive runs needed to be confirmed.

In this study, a textile azo-dye, orange G (OG), was chosen as a model compound. Many studies about AOPs (i.e. Fenton, photo-Fenton and TiO_2 photocatalysis) used to employ OG as model mainly because it is a widely used dye, and resistant to conventional methods, like adsorption and physico-chemical and biological treatments, in sewage treatment plants.[23, 24] To our knowledge, little information on OG degradation kinetics and mechanism in heterogeneous nano-Co_3O_4/PS process is available from previous studies. Hence this study not only intended to examine the influence of the experimental conditions (i.e. dosages of nano-Co_3O_4 and PS, catalyst particle size, pH and temperature), but also aimed to propose the degradation pathways of OG in nano-Co_3O_4/PS process. The primary reactive oxidants in nano-Co_3O_4/PS process were clarified. This study also tried to assess the stability of nano-Co_3O_4 in successive runs and explore the causes of deactivation. Usually, a great amount of salts and heavy metals are employed in various dyeing processes and the inorganic ions in dyeing wastewater may affect the efficiency of dye degradation reaction. Thus, the effects of several inorganic ions that commonly occur in real dye-containing wastewater on the OG degradation were

examined. The reactivity of three different sources of $SO4^{\bullet -}$ (i.e. potassium persulfate, sodium persulfate and Oxone®) in the presence of nano-Co_3O_4 was compared quantitatively for the first time.

2 Experimental

2.1 Reagents and materials

OG (98%), $Co(NO_3)_2 \cdot 6H_2O$, N-cetyl-N,N,N-trimethyl ammonium bromide (CTAB), $(CH_3CH_2)_3N$ (TEA), NaH_2PO_4 (99%), Na_2HPO_4 (98%), $Na_2S_2O_8$ (98%), potassium persulfate, sodium persulfate and Oxone® were all analytical grade and purchased from Sigma-Aldrich. Methanol (99.7%), ethanol (99.5%) and t-butyl alcohol (TBA, 99.5%) were both chromatographic pure and purchased from Sigma-Aldrich. Commercial CoO, Co_3O_4 and Co_2O_3 powder (97%), $NaNO_3$, NaCl, $NaHCO_3$, $Co(NO_3)_2$, $Fe(NO_3)_2$ and $Mn(NO_3)_2$ was from Sinopharm Chemical Reagent Co., China, 5,5-dimethyl-1-pyrrolidine N-oxide (DMPO) from J&K Chemical Co. All reagents were used as received, without further purification. The aqueous solutions were prepared by using Milli-Q water (resistivity ≥18.2 mΩ • cm).

2.2 Preparation and characterization of nano-Co_3O_4

Nano-Co_3O_4 particles were prepared as described by Zhou et al. [19], as shown in Text S1 in the SI. The morphology of nano-Co_3O_4 was determined using transmission electron microscopy (TEM, Model JEM-2011, Japan). Its crystal structure was characterized by X-ray diffractometer (XRD, D8 Advance, Bruker, Germany) with Cu Kα radiation (λ = 1.5418) in the 2θ scanning range from 15 to 70°. Zeta potentials at different pH were determined with a zeta analyzer (Zetasizer Nano, Malvern

Instruments Ltd., UK). X-ray photoelectron spectroscopy (XPS) measurements were performed on a PHI 5000C ESCA System with Al Kα source. All the binding energies were referenced to the contaminant C1s peak at 284.6 eV of the surface adventitious carbon. The BET surface areas were measured with the N_2 gas adsorption method on an ASAP analyzer (Micromeritics, USA). Prior to the adsorption-desorption measurements, the fresh catalyst was degassed at 300 ^{o}C in a N_2 flow for 2 h.

2.3 Experimental procedures

Batch experiments were conducted to explore the influences of initial pH, PS and nano-Co_3O_4 dosages, diameter of catalysts, pH and temperature on the performance of OG degradation. The experiments were performed open to the air and in a series of 500-mL borosilicate glass jars that were placed in a water bath to keep temperature constant. The solution was mixed at 300 rpm using a magnetic stirrer. With this stirring intensity, the catalyst could be evenly distributed in the solution. pH of the reaction solution was adjusted to predetermined value with NaOH or $HClO_4$. At the given time intervals, the samples aliquots were collected with syringes and mixed immediately with appropriate amounts of methanol to quench any further oxidation reactions.[8] The samples were filtered through a 0.22 μm membrane filter before measurement. All experiments were run in duplicates, and all points in the figures are the mean of the results and error bars represent standard deviation of the means.

For TOC measurement, sodium thiosulfate was chosen as the quencher to minimize any interference of quenching agent in TOC analysis. In the consecutive runs, the used catalyst was collected by filtration, rinsed with Milli-Q water for

several times, and then dried in vacuum at 40 ^{o}C for 12 h. Then, 2.0 mM PS was added with dry catalyst to the fresh OG-containing solution to initiate the next treatment.

The details of the experiments to assess the leaching test of nano-Co_3O_4 and the catalytic performance of dissolved Co ions were presented in Text S2 in SI. Quenching experiments were conducted with the addition of methanol and TBA for identifying the primary radical species. Electron paramagnetic resonance (EPR) experiments were performed using DMPO as spin-trapping agent, as shown in Text S3.

2.4 Analytical methods

The concentration of OG was analyzed with a Purkinje TU-1902 automatic scanning UV-Vis spectrophotometers with a spectrometric quartz cell (1 cm). The maximum absorbance wavelength of OG was observed at 478 nm. The concentrations of leached Co ions were determined by ICP-AES (Agilent 4200) after microwave digestion in the mixture of nitric acid and hydrogen peroxide. Total organic carbon (TOC) was monitored using a Shimadzu TOC analyzer (model TOC-VCPN, Japan) to identify the mineralization of OG. EPR experiments were performed on a Bruker A200 spectrometer (Germany). The UPLC-QTOF-MS was used to detect the intermediates of OG degradation. In this study, the mass spectrometer was operated in the *m/z* 50-500 range for LC-MS. Samples were eluted at 0.5 mL min^{-1} through a Acquity UPLC BEH C18 column (2.1 mm *100 mm, 1.7 μm) with the following gradient: from 1/99 (acetonitrile/0.2% formic acid) to 95/5 in 10 min, which was then

maintained for 3 min.

3 Results and discussion

3.1 Characterization of nano-Co_3O_4

TEM images of nano-Co_3O_4 before and after catalytic reaction in five successive runs are shown in Fig. S1(a) and (b), respectively. The virgin catalysts with an average diameter of 50 nm were mostly quasi-spherical. The morphology of spent Co_3O_4 nanoparticles remained virtually unchanged after five successive runs. Fig. S2 presented the XRD patterns of nano-Co_3O_4 before and after use for five times. Peaks of virgin and spent nano-Co_3O_4 appeared at $2\theta=18.9^o$, 31.2^o, 36.7^o, 38.5^o, 44.7^o, 55.7^o, 59.2^o and 65.0^o, which matched well with the standard XRD pattern of Co_3O_4 (JCPDS No. 47-1049) [25, 26], indicating that after five successive runs the main crystalline for nano-Co_3O_4 remained unchanged. N_2 adsorption-desorption isotherms were employed to study the surface area of virgin nano-Co_3O_4 and its spent counterpart after five successive runs. The BET surface areas were 18.1 and 17.8 m^2 g^{-1} for the virgin and spent nano-Co_3O_4, respectively.

The surface chemical composition and oxidation state of the virgin and spent nano-Co_3O_4 was investigated by XPS (Fig. 1). The XPS survey (0-1300 eV) in Fig. 1(A) shows the presence of oxygen and cobalt for nano-Co_3O_4. Fig. 1(B) shows the high resolution spectrum of the Co2p peak for the catalyst. One can see the presence of the two spin orbit components of Co (Co2p $_{3/2}$ at 780.1 eV and Co $2p_{1/2}$ at 795.5 eV) and the presence of associated shake-up satellites at higher energy (789.0 and 804.5 eV) for both Co peaks [29]. The energy between the $Co2p_{1/2}$ and $Co2p_{3/2}$ peaks for

186 nano-Co_3O_4 is 15.4 eV, and it is in agreement with that previously reported for
187 Co_3O_4.[27, 28] The satellite peaks in the Co2p spectra are an important signal for
188 distinguishing the bonding valence of cobalt oxide compounds. The lower intensity of
189 the shake-up satellites at 9 eV from the main spin-orbit components in Fig. 1(B) has
190 identified the cobalt in as-prepared catalyst was Co_3O_4 and not CoO.[27, 28] For
191 nano-Co_3O_4, the peak of Co $2p_{3/2}$ level was deconvoluted into two peaks concentrated
192 on at binding energy of 780.3 eV and 785.2 eV (Fig. 1(C)), which can be assigned to
193 surface Co(III) and Co(II) species [29], respectively. The recording of a weak signal at
194 binding energy of 789.8 eV indicates the presence of surface Co(II) species.
195 Quantitative analyses of the Co $2p_{3/2}$ XPS spectra can give the surface cobalt
196 compositions of the samples. Apparently, the surface Co(III)/Co(II) molar ratio (3.68)
197 of virgin Co_3O_4 was lower than that (3.82) used after 5 times. As shown in Fig. 1(D),
198 the observed position around 530 eV was the typical XPS spectrum of O1s region.
199 The O1s peak was deconvoluted into three spectral bands at 529.6, 530.6 and 532.9
200 eV in the virgin nano-Co_3O_4. The most intense peak at 529.6 eV was attributed to the
201 lattice oxygen (O_{latt}) in the metal oxide.[29] The 530.6 eV of binding energy was due to
202 the hydroxide (Co-OH) in the surface hydroxyls [29], and the relatively small peak at
203 532.9 eV represented physically adsorbed H_2O [30, 31]. Based on the XPS analysis, the
204 intensity of adsorbed water molecules in the spent nano-Co_3O_4 increased, although the
205 catalyst was dried in the vacuum oven for 12 h before XPS analysis.

206 **3.2 Effect of reaction conditions**

207 **3.2.1 Effects of Co_3O_4 particle size**

In order to compare the catalytic performance of nano-Co_3O_4 to that of commercial Co_3O_4 powder, both the nano-Co_3O_4 about 50 nm and Co_3O_4 powder with particle size of 5 μm were applied for activation of PS. Negligible OG was degraded by PS alone (2.0 mM) (Fig. S3) and less than 2.5% of OG was removed by nano-Co_3O_4 (Fig. S4) or Co_3O_4 alone (2.0 g L^{-1}) (data not shown) over 3 h. The addition of 0.5 g L^{-1} nano-Co_3O_4 to PS solution resulted in a very rapid and pronounced degradation of OG with 90.7% removal in 3 h at pH 7.0, indicating that nano-Co_3O_4 could activate PS effectively to initiate OG oxidation. In Co_3O_4/PS process, only 38.7% of OG was removed (Fig. 2). The higher catalytic performance of nano-Co_3O_4 might derive from its smaller particle size and higher surface area. Therefore, the specific rate constant (k_{SA}), yielded from the normalization of k (s^{-1}) data to the catalyst surface area (Eq. 1), is of great help in investigating the reactivity of catalysts.

$$k_{SA}=k/S_{BET} \quad (1)$$

where k_{SA} is the specific reaction rate constant (g m^{-2} s^{-1}) of OG removal, and S_{BET} is the surface area of catalyst (m^2 g^{-1}). The obtained close k_{SA} values for Co_3O_4 and nano-Co_3O_4 are 9.18×10^{-6} and 1.23×10^{-5} g m^{-2} s^{-1} (Table S1), respectively, indicating that the catalytic active sites available to PS depended largely on the catalyst surface area.[32]

3.2.2 Effect of nano-Co_3O_4 dosage

Fig. 3(a) illustrated the OG degradation by nano-Co_3O_4 activated PS at various nano-Co_3O_4 dosages. The OG degradation well followed exponential rate law,

indicating that the reaction was a pseudo-first-order ($R^2 > 0.998$) with respect to OG. The overall rate law for OG degradation can be expressed as Eq. 2,

$$-\frac{d[OG]}{dt} = k[OG] \quad (2)$$

where [OG] is the OG concentration at any specific time t and k (s^{-1}) is the pseudo-first-order degradation rate constant. The k (s^{-1}) rapidly increased linearly from 6.3×10^{-5} s^{-1} to 8.58×10^{-4} s^{-1} as the catalyst dosage increased from 0.1 g L^{-1} to 2.0 g L^{-1}. The significantly enhanced degradation could be attributed to the increased production of active radical species after introduction of the catalyst.[22, 33] A linear relationship was established between k (s^{-1}) and nano-Co_3O_4 dosage, as shown in the inset of Fig. 3(a). Similar linear formula were also reported in prior studies that cobalt-MCM_{41} activated PS to degrade caffeine [34], nano-Co_3O_4 activated H_2O_2 to decompose 2-chlorophenol [35] and Fe_3O_4 nanoparticles activated PMS to degrade acetaminophen [22].

3.2.3 Effect of PS dosage

The effect of variable PS concentration on the transformation of OG was studied in the presence of nano-Co_3O_4, as shown in Fig. 3(b). The increased dosage of PS from 0.5 to 2.0 mM and then to 4.0 mM understandably accelerated the degradation of OG with the k (s^{-1}) increasing from 7.5×10^{-5} to 3.57×10^{-4} s^{-1}. A linear relationship could be established between k (s^{-1}) and PS dosage in the range of 0.5-2.0 mM, as shown in the inset of Fig. 3(b), which indicated that the availability of PS was the limiting factor controlling the yield of radicals at a low PS dose. However, the PS contribution became considerably less important with further increasing the dosage of

PS from 2.0 mM to 4.0 mM, indicating that the active sites of fixed catalyst concentration gradually became the limiting factor. Similar phenomenon was also observed in Fe_3O_4 nanoparticles activating PMS to degrade acetaminophen [22].

3.2.4 Effects of initial pH

The effect of initial pH on OG degradation in nano-Co_3O_4/PS system is presented in Fig. 4(a). The OG adsorption onto nano-Co_3O_4 (Fig. S2) and oxidation by PS alone (Fig. S3) was less than 5% at pH 3.0-10.0, which indicated the adsorption by nano-Co_3O_4 and the oxidation by PS alone could be ignored in the evaluation of pH effect. As pH increased from 3.0 to 9.0, the k (s^{-1}) dramatically climbed from 1.35×10^{-4} s^{-1} to 3.18×10^{-4} s^{-1}, as shown in the inset of Fig. 4(a). With further increasing pH from 9.0 to 10.0, the k (s^{-1}) dropped from 3.18×10^{-4} s^{-1} to 2.45×10^{-4} s^{-1}. This could be attributed to the zeta potentials and surface charges of the catalysts. The point of zero charge (PZC) was determined to be around 8.5 for nano-Co_3O_4 catalyst (Fig. S5). When nano-Co_3O_4 was dispersed in water then the surface became cationic in nature, which would increase the more coverage of hydroxyl groups (-OH) from H_2O. Pu et al. reported that the uncharged surface hydroxyl groups of nano-Co_3O_4 were the main active sites in promoting persulfate decomposition to generate sulfate radicals $SO_4^{\bullet-}$.[36] Thus with increasing pH from 3.0 to 9.0, the kinetics of OG degradation sharply increased and reached it maximum at the pH near PZC. In addition, at an acidic condition, the H-bond formation between H^+ and the O−O group of $S_2O_8^{2-}$ would be significant, thus hindering the reaction between $S_2O_8^{2-}$ and positively charged catalyst surface [22]. When the solution pH was higher than PZC, the

catalyst surface became anionic and had a higher electronic force to repel the negative PS anion, so that less PS could reach the catalyst surface and OG degradation was decreased from pH 9.0 to 10.0.

The degradation of OG occurs on the catalyst surface (i.e., heterogeneous reaction) and/or in the bulk solution (i.e., homogeneous reaction). Which is the main process, heterogeneous nano-Co_3O_4/PS or homogeneous Co/PS? To clarify the mechanism, the concentration of dissolved Co ions leached from nano-Co_3O_4 catalyst at different pH was measured and the results are presented in Fig. 4(b). It is shown that under acidic condition, Co dissolved slowly from nano-Co_3O_4, reaching a value of 0.59 mg L^{-1} and 0.25 mg L^{-1} after 3 h at pH 3.0 and 5.0. Thus, nano-Co_3O_4 was slightly unstable under acidic condition. While at neutral or alkaline condition (pH 7.0, 9.0 and 10.0), dissolved Co was always below 0.05 mg L^{-1}, thus very limited Co dissolved from nano-Co_3O_4. The results were consistent with that of Dionysiou group [13] and Chen et al [20].

To evaluate the catalytic contribution from dissolved Co, homogeneous experiments with introduction of Co^{2+} into PS solution were conducted. As can be observed from Fig. 4(c), the degradation rate of OG was much faster when nano-Co_3O_4 was added. Thus it can be concluded safely that the main catalytic effect is caused by nano-Co_3O_4, not dissolved Co ions, whether at acidic or neutral pH. The heterogeneous catalysis of nano-Co_3O_4 was especially prominent under neutral pH, since its homogeneous counterpart was limited owing to the low concentration of dissolved Co ions. Most dyestuff wastewaters are neutral since they usually contain

large amount of buffer salts.[20] Thus the nano-Co_3O_4/PS system is quite acceptable from application point of view due to its very low dissolution of Co ions and high reactivity.

3.2.5 Effect of temperature

The kinetics of OG degradation by PS in the presence of nano-Co_3O_4 at 15-35 ^oC is depicted in Fig. S6. It is clearly seen that the reaction temperature positively affected the rate of OG degradation. The k (s^{-1}) increased from 1.48×10^{-4} s^{-1} to 3.52×10^{-4} s^{-1} with temperature increasing from 15 ^oC to 35 ^oC. Furthermore, the activation energy (E_a) was determined by plotting ln$k$ against 1/T, according to Arrhenius equation (Eq. 3):

$$\ln k = \ln A - \frac{E_a}{RT} \quad (3)$$

where k is the rate constant (s^{-1}), R is the universal gas constant (8.314 J $(mol\ K)^{-1}$) and A is a constant. The E_a value for nano-Co_3O_4/PS/OG system was determined to be 42.0 kJ mol^{-1}. This E_a value was much lower than that observed in PS/Fe_3O_4 process for p-nitroaniline degradation (65.6 kJ mol^{-1}) [37] and that in nZVI/PS process for 2,4-dichlophenol removal (91.5 kJ mol^{-1}) [38].

3.3 Identification of primary reactive oxidants in nano-Co_3O_4/PS process

It has been reported that two different reactive oxidants (i.e., $SO_4^{\bullet-}$ and •OH) can be generated for the catalyst-mediated decomposition of PS [39, 40], as shown in Eqs. 4-9. Owing to the high rate constants with $SO_4^{\bullet-}$ (2.5×10^7 $M^{-1}s^{-1}$ [41]) and •OH (9.7×10^8 $M^{-1}s^{-1}$ [42]), methanol is an effective quencher for both $SO_4^{\bullet-}$ and •OH. Due to the high rate constant with •OH (6.0×10^8 $M^{-1}s^{-1}$ [41]) and the much slower rate constant with SO_4

318 $^{\bullet-}$ (8.0×10^5 $M^{-1}s^{-1}$ [42]), TBA is an effective quencher for •OH but not for $SO_4^{\bullet-}$. Based
319 on these properties, the quenching experiments with methanol and TBA could allow
320 us to differentiate between the contribution of $SO_4^{\bullet-}$ and •OH.

321 $$S_2O_8^{2-} + \equiv Co_3O_4 \rightarrow 2SO_4^{\bullet-} \quad (4)$$

322 $$SO_4^{\bullet-} + OH^- \rightarrow \bullet OH + SO_4^{2-} \qquad k_1=6.5\times10^7\ [33] \quad (5)$$

323 $$SO_4^{\bullet-} + SO_4^{\bullet-} \rightarrow S_2O_8^{2-} \qquad k_2=8.1\times10^8\ M^{-1}\ s^{-1}\ \ pH=5.8\ [43] \quad (6)$$

324 $$5.0\times10^8\ M^{-1}\ s^{-1}\ \ pH=5.0$$

325 $$4.8\times10^8\ M^{-1}\ s^{-1}\ \ pH=4.8$$

326 $$SO_4^{\bullet-} + S_2O_8^{2-} \rightarrow S_2O_8^{\bullet-} + SO_4^{2-} \qquad k_3=5.5\times10^5\ M^{-1}\ s^{-1}\ [44] \quad (7)$$

327 $$SO_4^{\bullet-} + \bullet OH \rightarrow HSO_5^- \qquad k_4=1.0\times10^{10}\ M^{-1}\ s^{-1}\ [45] \quad (8)$$

328 $$SO_4^{\bullet-} + H_2O \rightarrow HSO_4^{2-} + \bullet OH \qquad k_5=8.3\ M^{-1}\ s^{-1}\ [44] \quad (9)$$

329 In the presence of TBA

330 $$HO\bullet + (CH_3)_3COH \rightarrow \text{product} \qquad k_6 = 6.0\times10^8\ [42] \quad (10)$$

331 $$SO_4^{\bullet-} + (CH_3)_3COH \rightarrow \text{product} \qquad k_7 = 8.0\times10^5\ [41] \quad (11)$$

332 In the presence of methanol

333 $$HO\bullet + CH_3OH \rightarrow \text{product} \qquad k_8 = 9.7\times10^8\ [42] \quad (12)$$

334 $$SO_4^{\bullet-} + CH_3OH \rightarrow \text{product} \qquad k_9 = 2.5\times10^7\ [41] \quad (13)$$

335 Fig. S7 shows the inhibition effect of TBA and methanol on the degradation of
336 OG in nano-Co_3O_4/PS process. With the addition of 10 mM methanol (100 times of
337 the initial OG concentration), the removal of OG decreased remarkably from 90.7% to
338 30.7%. Meanwhile, the degradation of OG was decreased from 90.7% to 44.9% with
339 the addition of 10 mM TBA. Based on the inhibition effect of methanol and TBA on

OG degradation, it could be concluded that both the $SO_4^{\bullet-}$ and •OH were the primary reactive oxidants in nano-Co_3O_4/PS process [20, 40].

An attempt with EPR experiments was made to consolidate the presence of $SO_4^{\bullet-}$ and •OH in nano-Co_3O_4/PS process. DMPO was selected as the spin trapping agent in EPR experiments. $SO_4^{\bullet-}$ and •OH could be detected by measuring the signals of DMPO-OH adducts and DMPO-SO_4 adducts, respectively.[4, 46] As seen in Fig. 5(a), when pure water was tested with addition of DMPO, no peaks were identified, suggesting that no spins were captured. Characteristic signals of 5,5-dimethylpyrroline-(2)-oxyl-(1) (DMPOX) with an intensity ratio of 1:2:1:2:1:2:1 were identified with the addition of 0.1 M DMPO to the PS solution, indicating the oxidation of DMPO by PS (Scheme S1). When nano-Co_3O_4 was added together with DMPO and PS, both $SO_4^{\bullet-}$ and •OH were identified with the characteristic peaks of DMPO-HO and DMPO-SO_4 adducts, respectively (Fig. 5(b)). The special hyperfine coupling constants (a(N) 1.49 mT, a(H) 1.49 mT, all ±0.05 mT, obtained by simulation) were consistent with that of DMPO-OH adducts, while the special hyperfine coupling constants (a(N) 1.38 mT, a(H) 1.02 mT, a(H) 0.14 mT, a(H) 0.08 mT, all ±0.05 mT, obtained by simulation) were in accordance with that of DMPO-SO_4 adducts. But the intensity of DMPO-OH signals was much stronger than that of DMPO-SO_4 due to the fast transformation from DMPO-SO_4 to DMPO-OH via nucleophilic substitution (Scheme S1).[46]

3.4 Decolorization, degradation pathways and mineralization of OG in nano-Co_3O_4/PS process

The UV-Vis spectra of OG decolorization evolution by nano-Co_3O_4/PS is presented in Fig. S8. The absorption spectra of OG were scanned in the range of 300-600 nm. The spectrum of light absorption by OG solution before reaction consists of two main peaks at 328 and 478 nm, plus a shoulder peak at 421 nm, which was consistent with the observations of Xu and Li [47] and Xiong et al [40]. The peak at 478 nm is attributed to the absorption of the π-π* transition related to the –N=N– group, while additional bands at 328 nm are assigned to its aromatic ring in the OG molecule. As the reaction proceeded, the two characteristic absorption peaks at 328 and 478 nm decreased dramatically and almost disappeared after 180 min, showing that the chromophore and conjugated system were completely destroyed.

Although efforts have been made to explore OG degradation pathways in sonolysis[48] and Fenton[49,50] processes, the mechanisms of OG degradation in nano-Co_3O_4/PS process were kept unknown. Thus in this study the byproducts were identified by LC-MS and the mechanistic pathways were depicted in Fig. 6. The retention time and formula for each byproduct was listed in Table S2. Most of the byproducts had lower molecular weights and earlier retention times than their parent molecules. The proposed structures of degradation products revealed that $SO_4^{\bullet-}$ and •OH initially attacks the aromatic ring, leading to the loss of characteristic fragments of 80 (SO_3H), 77 (phenyl), 16 (OH), and 104 (phenyl–N=N group). Then the further attacks by radicals resulted the formation of various hydroxyl substituted intermediates and quinone end products, as shown in Fig. 6. Previous studies have confirmed that azo chromophore is the essential functional group responsible for the

color of azo dyes, thus the loss of 77 (phenyl) and 104 (phenyl–N=N group) directly lead to the decoloration of OG in nano-Co_3O_4/PS process.

The influence of nano-Co_3O_4 on the mineralization of OG by PS was determined by varying the dosage of PS from 2.0 to 4.0 mM with a fixed nano-Co_3O_4 dosage of 0.5 g L^{-1} and the results are shown in Fig. S9. Without nano-Co_3O_4, no mineralization was observed when PS was dosed at 2.0 mM and 1.1% of OG was mineralized when PS was dosed at 4.0 mM. With the introduction of nano-Co_3O_4, OG mineralization rate increased remarkably from 5.6% to 16.4% in 3 h by increasing PS dosage from 2.0 mM to 4.0 mM. Therefore, the application of nano-Co_3O_4 significantly increased not only the removal rate but also the mineralization of OG.

3.5 Stability and reusability of nano-Co_3O_4

Since the stability and reusability of catalyst are critical in catalyzed reactions, the stability of nano-Co_3O_4 was investigated by reusing it in five successive experiments under the same reaction conditions and the results are shown in Fig. 7. The removal efficiency of OG dropped progressively from 100% to ~64.2% during five successive runs after 3 h of reaction, probably due to the leaching of Co from the catalyst surface determined in the former section, which means that the degradation rate of OG was gradually reduced by repeated reuse of the catalyst, thereby prolonging the time for complete removal of OG. After 5 h of reaction, OG was almost completely removed by the reused catalyst, which indicated the possibility of using the catalyst for a longer operation time. Another cause for the decreasing performance of nano-Co_3O_4 may be the reduced number of Co(II) and Co(II)-OH on

406 the surface of catalyst. The standard redox potentials of $Co(H_2O)_6^{3+}/Co(H_2O)_6^{2+}$ and
407 $Co(OH)_3/Co(OH)_2$ are 1.92 V and 0.17 V [51] respectively, while that of $\bullet OH/OH^-$ and
408 $SO_4^{\bullet -}/SO_4^{2-}$ is 2.8 V and 2.6-3.1 V [39]; hence, the transfer of electrons from Co(II)
409 to $\bullet OH$ and $SO_4^{\bullet -}$ radicals is thermodynamically favored. The XPS results also
410 confirmed the oxidation of Co(II) and Co(II)-OH to Co(III) and Co(III)-OH. The
411 surface Co(III)/Co(II) molar ratio (3.68) of virgin nano-Co_3O_4 was lower than that
412 (3.82) used after 5 times due to the gradual formation of Co(III) and Co(III)-OH from
413 Co(II) and Co(II)-OH, as shown in Fig. 1(C). In order to consolidate this result,
414 experiments were performed with commercial CoO, Co_3O_4 and Co_2O_3 as
415 heterogeneous catalysts (Fig. S10). All the commercial powders were of micrometer,
416 so as to exclude the size effect of nano-Co_3O_4. It was interesting to observe that CoO
417 possesses the highest catalytic capability, Co_3O_4 in the medium, and Co_2O_3 the lowest.
418 Thus it can be safely concluded that the main catalytic sites on nano-Co_3O_4 was Co(II)
419 and Co(III)-OH. However, it should be noted that Co_2O_3 also possesses a slight
420 catalytic effect on OG oxidation by PS, possibly due to the conversion between Co(III)
421 to Co(II).[52] Therefore, the depression in the catalytic performance may be mainly
422 associated with the reduced number of active sites on nano-Co_3O_4 by the oxidation of
423 sulfate- and hydroxyl-radicals and the leaching of cobalt ions.

424 **3.6 Effect of co-existing water matrix chemicals**

425 Textile effluents contain a variety of azo-dyes of various structures, lots of salts
426 and various metal ions. NaCl, $NaNO_3$, Na_2CO_3 and $NaHCO_3$ salts are generally added
427 to dye baths for improving the fixation of dyes on fabrics, and to adjust the ionic

strength of the dye baths.[53] According to one estimate, about 30% metal complexed dyes are used in dyeing wool and 40 % for dyeing polyamide.[54] Therefore, dyes are considered a major source of various metals, including Cd, Cr, Co, Cu, Hg, Ni, Mg, Fe and Mn that are discharged in the raw textile effluents.[53] Thus the effects of Cl^-, NO_3^-, HCO_3^-, Co^{2+}, Fe^{2+} and Mn^{2+} ions on OG removal by nano-Co_3O_4/PS was studied. The experiments were conducted in the concentration range of 5-20 mM for Cl^- and HCO_3^- ions, and in the concentration range of 5 μM-10 mM for heavy metals.

The results indicated that OG degradation was not significantly influenced with 5 mM Cl^- ion. However, as the concentration of Cl^- ions increased to 10-20 mM, an inhibition was observed (Fig. 8(a)). It is thermodynamically feasible for $SO_4^{\cdot-}$ (2.50 V) to oxidize chloride ions (Cl^-) into less reactive chlorine species viz. $Cl_2/2Cl^-$ (1.40 V) [51] and $HOCl/Cl^-$ (1.48 V) [55]. The chemical reactions involved in (but not limited to) nano-Co_3O_4/PS system in the presence of Cl^- ions can be given as follows [56]:

$$SO_4^{\cdot-} + Cl^- \rightarrow SO_4^{2-} + Cl^{\cdot} \quad (14)$$

$$Cl^{\cdot} + Cl^- \rightarrow Cl_2^{\cdot-} \quad (15)$$

$$Cl_2^{\cdot-} + Cl_2^{\cdot-} \rightarrow Cl_2 + 2Cl^- \quad (16)$$

$$Cl_2 + H_2O \rightarrow HOCl + H^+ + Cl^- \quad (17)$$

$$HOCl \rightarrow H^+ + OCl^- \quad (18)$$

Therefore, the observed inhibition in the presence of 10-20 mM Cl^- is due to the consumption of sulfate radicals by Cl^- ions (Eq. 14-18) [57], and the formation of less reactive chlorine species Cl_2, HOCl, $Cl^{\cdot}$ and $Cl_2^{\cdot-}$ [55, 57].

The bicarbonate ion (HCO_3^-) is an efficient radical scavenger (Eqs. 19 and 20 [58]).

With increasing HCO_3^- from 0 to 20 mM, the OG removal dropped from 71% to 33% (Fig. 8(b)). The NO_3^- ions have no obvious effect on the performance of nano-Co_3O_4/PS process. With its concentration increasing from 5 mM to 20 mM, the removal of OG remained constant, as shown in Fig. 8(c).

$$SO_4^{\cdot-} + HCO_3^- \rightarrow SO_4^{2-} + CO_3^{\cdot-} + H^+ \quad (k_{10}=1.6\times10^6\ M^{-1}\ s^{-1}) \qquad (19)$$

$$\cdot OH + HCO_3^- \rightarrow CO_3^{\cdot-} + H_2O \quad (k_{11}=8.5\times10^6\ M^{-1}\ s^{-1}) \qquad (20)$$

Ferrous ions (Fe^{2+}) can rapidly activate persulfate to form sulfate radicals ($SO_4^{\cdot-}$) at a high rate constant (k) of $2.7\times10\ M^{-1}\ s^{-1}$. However, a stronger interaction (k = $4.6\times10^9\ M^{-1}\ s^{-1}$) between Fe^{2+} and sulfate radicals was reported.[59] Thus, Fe^{2+} might be converted simultaneously by both PS and sulfate radicals, and the final reaction product (SO_4^{2-}) remained in the system, as shown in Fig. 8(d). The reaction equations were as follows (Eqs. 21-22).

$$Fe^{2+} + S_2O_8^{2-} \rightarrow Fe^{3+} + SO_4^{2-} + SO_4^{\cdot-} \quad k_{12}=2.7\times10\ M^{-1}\ s^{-1} \qquad (21)$$

$$Fe^{2+} + SO_4^{\cdot-} \rightarrow Fe^{3+} + SO_4^{2-} \quad k_{13}=4.6\times10^9\ M^{-1}\ s^{-1} \qquad (22)$$

Therefore, 1.0 mM was found to be the optimized iron concentration with 87% of OG removal in 90 min (Fig. 8(d)). When the Fe^{2+} concentration was increased to 10 mM, only 60.5% of OG was removed due to the consumption of generated radicals by excess Fe^{2+} ions.

Experimental results showed that Co^{2+}/PS system was more efficient for OG dissipation in relative to Fe^{2+}/PS system (Fig. 8(e)). The lowest Co^{2+} concentration used for PS activation was orders of magnitude lower than that of Fe^{2+}, confirming Co^{2+} was a better activator for PS. The degradation of OG increased appreciably with

increasing Co^{2+} concentration. For example, removal rate was found to be 91.5%, 100% and 100% for Co^{2+} of 5 μM, 10 μM and 1 mM, respectively. It has been proposed that Co^{2+} acts as a catalyst during PS activation (Eq. 23), and Co^{2+} regeneration occurs via Co^{3+} reduction [52]. However, it has been reported that excess Co^{2+} might also scavenge $SO_4^{\cdot -}$ (Eq. 24), which was also confirmed by this study. With increasing the concentration of Co^{2+} to 10 mM, the decomposition of OG by nano-Co_3O_4/PS was suppressed.

$$Co^{2+} + S_2O_8^{2-} \rightarrow Co^{3+} + SO_4^{2-} + SO_4^{\cdot -} \quad (23)$$

$$Co^{2+} + SO_4^{\cdot -} \rightarrow Co^{3+} + SO_4^{2-} \quad (24)$$

With increasing the concentration of Mn^{2+} from 5 μM to 10 mM, the degradation of OG was sharply suppressed (Fig. 8(f)). During the reaction, Mn^{2+} was also oxidized by PS or radicals and precipitated as MnO_2.[60] Thus the Mn^{2+} played a role of scavenger for reactive radical species and competitor to the target organics in nano-Co_3O_4/PS system.

In summary, the anions and Mn^{2+} have no or some inhibition on the performance of nano-Co_3O_4/PS system due to their scavenging effect on the reactive radical species ($SO_4^{\cdot -}$ or OH). While both the ferrous and cobalt ions with lower concentration enhanced the degradation of OG by promoting the production of active radicals. But the higher concentration of ferrous and cobalt ions played a role of scavenger for reactive radical species and competitor to the target organics in nano-Co_3O_4/PS system.

3.7 Comparison with the nano-Co_3O_4/PMS and nano-Co_3O_4/NaPS systems

494 Nano-Co_3O_4 species are known to activate peroxymonosulfate and persulfate to
495 generate $SO_4^{\bullet-}$ and •OH for oxidation of organic compounds in water. Thus, the
496 performances of potassium persulfate (PS), which was used throughout this study in
497 above sections, sodium persulfate (NaPS) and Oxone® (PMS) were compared in
498 nano-Co_3O_4 related oxidation systems, i.e., nano-Co_3O_4/PMS, nano-Co_3O_4/PS and
499 nano-Co_3O_4/NaPS. Fig. 9 shows that nano-Co_3O_4/PMS displayed the best
500 performance for the decomposition of OG (93% removal) after 60 min, at which the
501 removal of OG in nano-Co_3O_4/PS and nano-Co_3O_4/NaPS processes were 56.8% and
502 46.1% respectively. This indicated that higher levels of radicals were generated in
503 nano-Co_3O_4/PMS than that in nano-Co_3O_4/PS and nano-Co_3O_4/NaPS.[61] However, this
504 finding was totally contrary to the results reported by Luo et al. [61], who found PS
505 produced higher amount of sulfate- and hydroxyl-radicals than PMS in the presence
506 of UV irradiation at 254 nm. It should be noted that the pH for PMS/UV and PS/UV
507 were 3.65 and 5.88 respectively in Luo's study and very different from that of 7.0 in
508 this study. In addition, the production of radicals may also have close relationship to
509 the activation methods. The investigation and discussion about the reactivity
510 discrepancy of PS, NaPS and PMS was not deep enough in this study and further
511 studies are needed.

512 **4 Conclusions**

513 Nano-Co_3O_4 exhibited good heterogeneous activity in nano-Co_3O_4/PS system
514 and low dissolved Co ions especially at neutral or alkaline conditions. The smaller
515 particle size of Co_3O_4, higher dosage of PS and catalyst, and higher temperature

promoted the degradation of OG in nano-Co_3O_4/PS system. Both $SO_4^{\bullet -}$ and $^{\bullet}OH$ were proved to be the primary oxidative species by EPR experiment and the quenching results with TBA and methanol. The byproducts of OG in nano-Co_3O_4/PS process were identified by LC-MS and the mechanistic pathways were proposed. The stability of nano-Co_3O_4 was acceptable, although a slight decline in the catalytic ability was observed due to the oxidation of surface Co(II) to Co(III) and the leaching of cobalt ions. The NO_3^-, Cl^-, HCO_3^-, and Mn^{2+} have no or some inhibited effect on the performance of nano-Co_3O_4/PS system due to their scavenging effect on the reactive radical species and competition with target organics for the oxidant. Fe^{2+} and Co^{2+} with lower concentration enhanced the degradation of OG by promoting the production of active radicals. The reactivity discrepancy of PS, NaPS and PMS followed the order of nano-Co_3O_4/PMS > nano-Co_3O_4/PS > nano-Co_3O_4/NaPS.

Acknowledgement

This work was supported by the National Natural Science Foundation of China (51508152), Natural Science Foundation of Jiangsu Province (BK20150812), the China Postdoctoral Science Foundation (2015M571660), the Fundamental Research Funds for the Central Universities (2014B12614) and the Priority Academic Program Development of Jiangsu Higher Education Institutions.

References

1. J. Y. Fang and C. Shang, *Environ. Sci. Technol.*, 2012, **46**, 8976.
2. R. L. Johnson, P. G. Tratnyek and R. O. Johnson, *Environ. Sci. Technol.*, 2008, **42**, 9350.

3. W. S. Chen and Y. C. Su, *Ultrason. Sonochem.*, 2012, **19**, 921.
4. O. S. Furman, A. L. Teel and R. J. Watts, *Environ. Sci. Technol.*, 2010, **44**, 6423.
5. S. Y. Yang, X. Yang, X. T. Shao, R. Niu and L. L. Wang, *J. Hazard. Mater.*, 2011, **186**, 659.
6. G. D. Fang, J. Gao, D. D. Dionysiou, C. Liu and D. M. Zhou, *Environ. Sci. Technol.*, 2013, **47**, 4605.
7. M. Ahmad, A. L. Teel and R. J. Watts, *Environ. Sci. Technol.*, 2013, **47**, 5864.
8. G. P. Anipsitakis and D. D. Dionysiou, *Environ. Sci. Technol.*, 2004, **38**, 3705.
9. T. Zhang, H. B. Zhu and J. P. Croue, *Environ. Sci. Technol.*, 2013, **47**, 2784.
10. Y. B. Ding, L. H. Zhu, N. Wang and H. Q. Tang, *Appl. Catal. B-Environ.*, 2013, **129**, 153.
11. G. P. Anipsitakis and D. D. Dionysiou, *Environ. Sci. Technol.*, 2003, **37**, 4790.
12. J. Fernandez, P. Maruthamuthu, A. Renken and J. Kiwi, *Appl. Catal. B-Environ.*, 2004, **49**, 207.
13. G. P. Anipsitakis, E. Stathatos and D. D. Dionysiou, *J. Phys. Chem. B*, 2005, **109**, 13052.
14. Y. H. Guan, J. Ma, Y. M. Ren, Y. L. Liu, J. Y. Xiao, L. Q. Lin and C. Zhang, *Water Res.*, 2013, **47**, 5431.
15. C. Cai, H. Zhang, X. Zhong and L. W. Hou, *J. Hazard. Mater.s*, 2015, **283**, 70.
16. S. N. Su, W. L. Guo, Y. Q. Leng, C. L. Yi and Z. M. Ma, *J. Hazard. Mater.*, 2013, **244**, 736.
17. Y. J. Yao, Y. M. Cai, G. D. Wu, F. Y. Wei, X. Y. Li, H. Chen and S. B. Wang, *J.*

Hazard. Mater., 2015, **296**, 128.

18. Y. Jiang, Y. Wu, B. Xie, Y. Xie and Y. T. Qian, *Mater. Chem. Phys.*, 2002, **74**, 234.

19. L. P. Zhou, J. Xu, H. Miao, F. Wang and X. Q. Li, *Appl. Catal. A-Gen.*, 2005, **292**, 223.

20. X. Y. Chen, J. W. Chen, X. L. Qiao, D. G. Wang and X. Y. Cai, *Appl. Catal. B-Environ.*, 2008, **80**, 116.

21. E. Saputra, S. Muhammad, H. Q. Sun, H. M. Ang, M. O. Tade and S. B. Wang, *J. Colloid Interf. Sci.*, 2013, **407**, 467.

22. C. Q. Tan, N. Y. Gao, Y. Deng, J. Deng, S. Q. Zhou, J. Li and X. Y. Xin, *J. Hazard. Mater.*, 2014, **276**, 452.

23. A. El-Ghenymy, F. Centellas, J. A. Garrido, R. M. Rodriguez, I. Sires, P. L. Cabot and E. Brillas, *Electrochim. Acta*, 2014, **130**, 568.

24. A. B. dos Santos, F. J. Cervantes and J. B. van Lier, *Bioresource Technol.*, 2007, **98**, 2369.

25. P. Shukla, H. Q. Sun, S. B. Wang, H. M. Ang and M. O. Tade, *Sep. Purif. Technol.*, 2011, **77**, 230.

26. P. H. Shi, R. J. Su, S. B. Zhu, M. C. Zhu, D. X. Li and S. H. Xu, *J. Hazard. Mater.*, 2012, **229**, 331.

27. D. Barreca, C. Massignan, S. Daolio, M. Fabrizio, C. Piccirillo, L. Armelao and E. Tondello, *Chem. Mater.*, 2001, **13**, 588.

28. Z. L. Chen, S. H. Chen, Y. H. Li, X. L. Si, J. Huang, S. Massey and G. L. Chen,

582 *Mater. Res. Bull.*, 2014, **57**, 170.

583 29. G. M. Bai, H. X. Dai, J. G. Deng, Y. X. Liu, F. Wang, Z. X. Zhao, W. G. Qiu and

584 C. T. Au, *Appl. Catal. A-Gen.*, 2013, **450**, 42.

585 30. C. H. Sun and J. C. Berg, *Adv. Colloid Interfac.*, 2003, **105**, 151.

586 31. P. H. Shi, X. F. Dai, H. G. Zheng, D. X. Li, W. F. Yao and C. Y. Hu, *Chem. Eng.*

587 *J.*, 2014, **240**, 264.

588 32. T. L. Johnson, M. M. Scherer and P. G. Tratnyek, *Environ. Sci. Technol.*, 1996,

589 **30**, 2634.

590 33. Y. H. Guan, J. Ma, X. C. Li, J. Y. Fang and L. W. Chen, *Environ. Sci. Technol.*,

591 2011, **45**, 9308.

592 34. F. Qi, W. Chu and B. B. Xu, *Appl. Catal. B-Environ.*, 2013, **134**, 324.

593 35. Q. Chang, K. J. Deng, L. H. Zhu, G. D. Jiang, C. Yu and H. Q. Tang, *Microchim.*

594 *Acta*, 2009, **165**, 299.

595 36. M. J. Pu, Y. W. Ma, J. Q. Wan, Y. Wang, M. Z. Huang and Y. M. Chen, *J. Colloid*

596 *Interf. Sci.*, 2014, **418**, 330.

597 37. Y. S. Zhao, C. Sun, J. Q. Sun and R. Zhou, *Sep. Purif. Technol.*, 2015, **142**, 182.

598 38. R. C. Li, X. Y. Jin, M. Megharaj, R. Naidu and Z. L. Chen, *Chem. Eng. J.*, 2015,

599 **264**, 587.

600 39. P. Avetta, A. Pensato, M. Minella, M. Malandrino, V. Maurino, C. Minero, K.

601 Hanna and D. Vione, *Environ. Sci. Technol.*, 2015, **49**, 1043.

602 40. X. M. Xiong, B. Sun, J. Zhang, N. Y. Gao, J. M. Shen, J. L. Li and X. H. Guan,

603 *Water Res.*, 2014, **62**, 53.

41. P. Neta, R. E. Huie and A. B. Ross, *J. Phys. Chem. Ref. Data* 1988, **17**, 1027.

42. G. V. Buxton, C. L. Greenstock, W. P. Helman and A. B. Ross, *J. Phys. Chem. Ref. Data*, 1988, **17**, 513.

43. P. Neta, R. E. Huie and A. B. Ross, *J. Phys. Chem. Ref. Data*, 1988, **17**, 1027.

44. X. Y. Yu, Z. C. Bao and J. R. Barker, *J. Phys. Chem. A*, 2004, **108**, 295.

45. U. K. Klaning, K. Sehested and E. H. Appelman, *Inorg. Chem.* , 1991, **30**, 3582.

46. G. S. Timmins, K. J. Liu, E. J. H. Bechara, Y. Kotake and H. M. Swartz, *Free Radical Bio. Med.*, 1999, **27**, 329.

47. X. R. Xu and X. Z. Li, *Sep. Purif. Technol.*, 2010, **72**, 105.

48. M. Q. Cai, M. C. Jin and L. K. Weavers, *Ultrason. Sonochem.*, 2011, **18**, 1068.

49. A. D. Bokare, R.C. Chikate, C. V. Rode and K. M. Paknikar, *Environ. Sci. Technol.* 2007, **41**, 7437.

50. M. Q. Cai , J. Su , Y. Z. Zhu , X.Q. Wei , M.C. Jin, H. J. Zhang , C.Y. Dong and Z.S. Wei, *Ultrason. Sonochem.*, 2016, **28**, 302.

51. J. G. Speight, *Lange's Handbook of Chemistry*, McGraw-Hill Education, New York, 2005.

52. Y. F. Ji, C. X. Dong, D. A. Kong and J. H. Lu, *J. Hazard. Mater.*, 2015, **285**, 491.

53. M. Imran, D. E. Crowley, A. Khalid, S. Hussain, M. W. Mumtaz and M. Arshad, *Rev. Environ. Sci. Bio.*, 2015, **14**, 73.

54. K. Hunger, *Industrial dyes-chemistry, properties, application*, VCH, New York, 2003.

55. Z. H. Wang, R. X. Yuan, Y. G. Guo, L. Xu and J. S. Liu, *J. Hazard. Mater.*, 2011,

626 **190**, 1083.

627 56. R. X. Yuan, S. N. Ramjaun, Z. H. Wang and J. S. Liu, *J. Hazard. Mater.*, 2011,

628 **196**, 173.

629 57. C. J. Liang, Z. S. Wang and N. Mohanty, *Sci. Total Environ.*, 2006, **370**, 271.

630 58. A. Ghauch and A. Tuqan, *Chem. Eng. J.*, 2012, **183**, 162.

631 59. C. S. Liu, K. Shih, C. X. Sun and F. Wang, *Sci. Total Environ.*, 2012, **416**, 507.

632 60. H. Akiho, S. Ito, H. Matsuda and T. Yoshioka, *Environ. Sci. Technol.*, 2013, **47**,

633 11311.

634 61. C. W. Luo, J. Ma, J. Jiang, Y. Z. Liu, Y. Song, Y. Yang, Y. H. Guan and D. J. Wu,

635 *Water Res.*, 2015, **80**, 99.

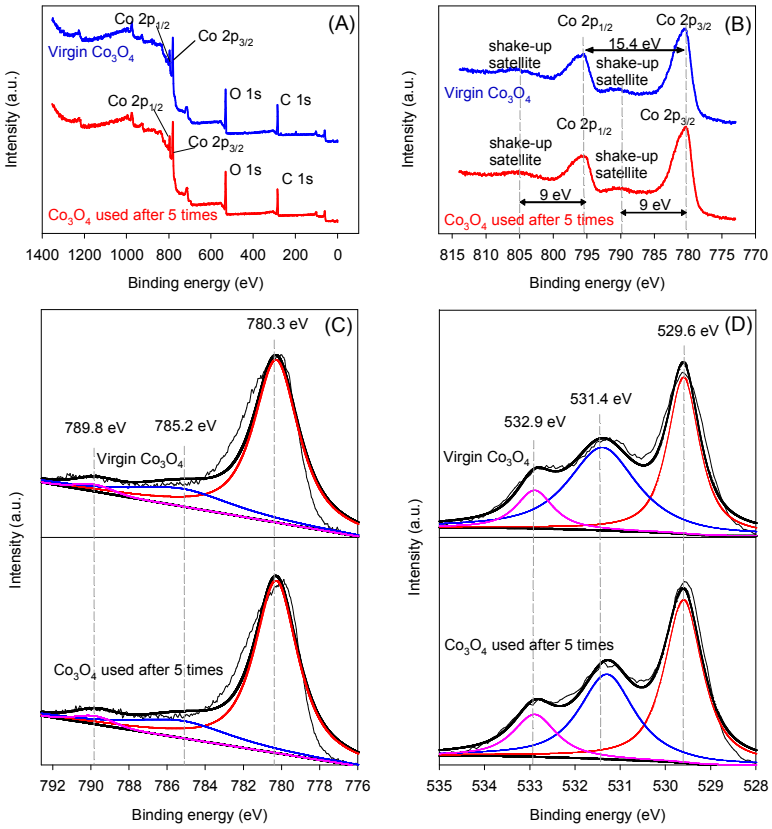

Fig.1 Survey spectra (A), Co 2p XPS spectra (B), Co $2p_{3/2}$ XPS spectra (C) and O 1s XPS spectra (D) of virgin and spent nano-Co_3O_4.

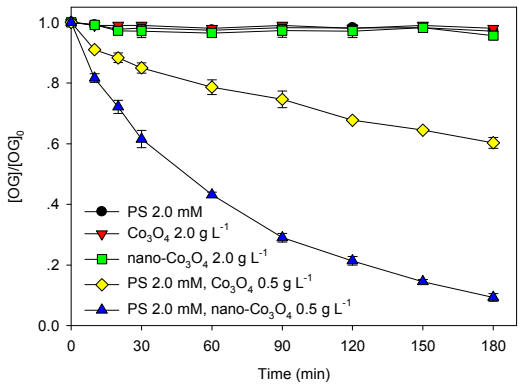

Fig. 2 Effect of catalyst particle size on OG degradation in Co_3O_4/PS and nano-Co_3O_4/PS processes. (Reaction conditions: [OG]=0.1 mM, pH=7.0±0.1, T=25 ^oC).

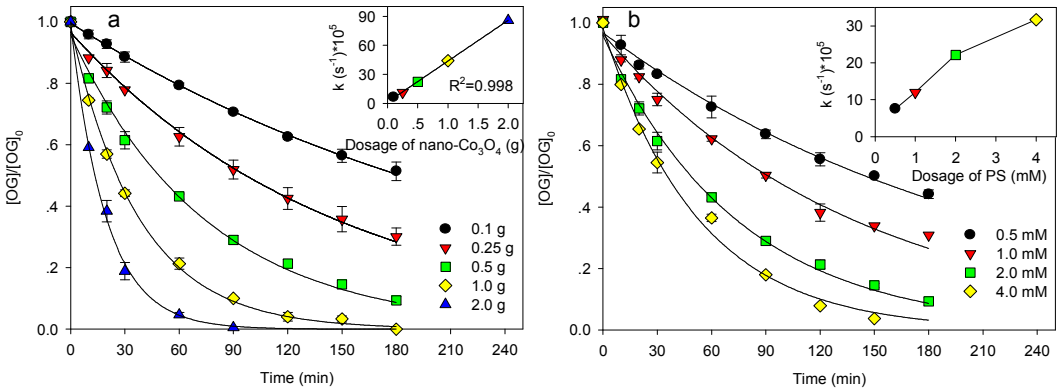

Fig. 3 (a) Effect of nano-Co_3O_4 dosage on OG degradation in nano-Co_3O_4/PS system. Inset indicates pseudo-first-order rate constants of OG degradation versus dosage of nano-Co_3O_4. (Reaction conditions: [OG]=0.1 mM, [PS]=2.0 mM, pH=7.0±0.1, T=25 ^oC). (b) Effect of PS dosage on OG degradation in nano-Co_3O_4/PS system. Inset indicates pseudo-first-order rate constants of OG degradation versus dosage of PS. (Reaction conditions: [OG]=0.1 mM, [nano-Co_3O_4]=0.5 g L^{-1}, pH=7.0±0.1, T=25 ^oC).

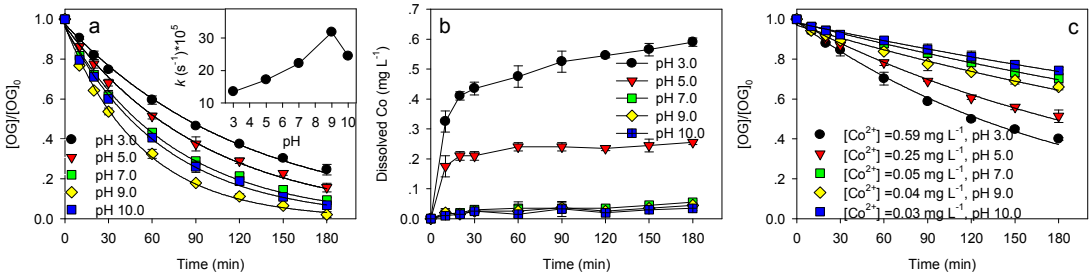

Fig. 4 (a) Degradation of OG in the nano-Co_3O_4/PS system at different pH. Inset indicates pseudo-first-order rate constants of OG degradation versus pH; (b) Dissolution of Co from nano-Co_3O_4 under various pH (Reaction conditions for (a-b): $[OG]_0$=0.1 mM, $[PS]_0$=2.0 mM, [nano-Co_3O_4]=0.5 g L^{-1}, T=25 ^oC). (c) Degradation of OG with homogeneous Co^{2+}/PS at various pH. The dosage of Co^{2+} was set according the maximum dissolved Co ions at the end of reactions in (b) (Reaction conditions for (c): $[OG]_0$=0.1 mM, $[PS]_0$=2.0 mM, T=25 ^oC).

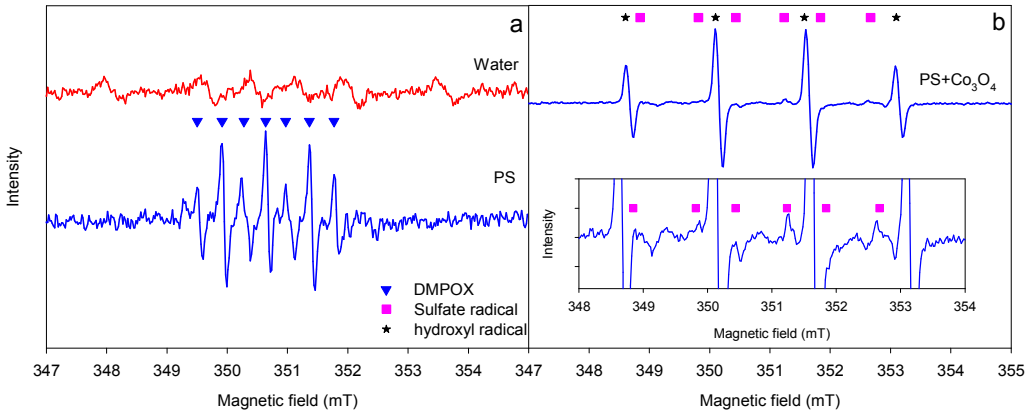

Fig. 5 EPR spectra obtained from ultrapure water, PS oxidative process and nano-Co_3O_4 activated PS oxidative process in the presence of DMPO. Reaction condition: $[PS]_0$=40 mM, $[Co_3O_4]_0$=0 or 5 g L^{-1}, $[DMPO]_0$≈0.1 M, pH=3.0±0.1, T=25 ^oC.

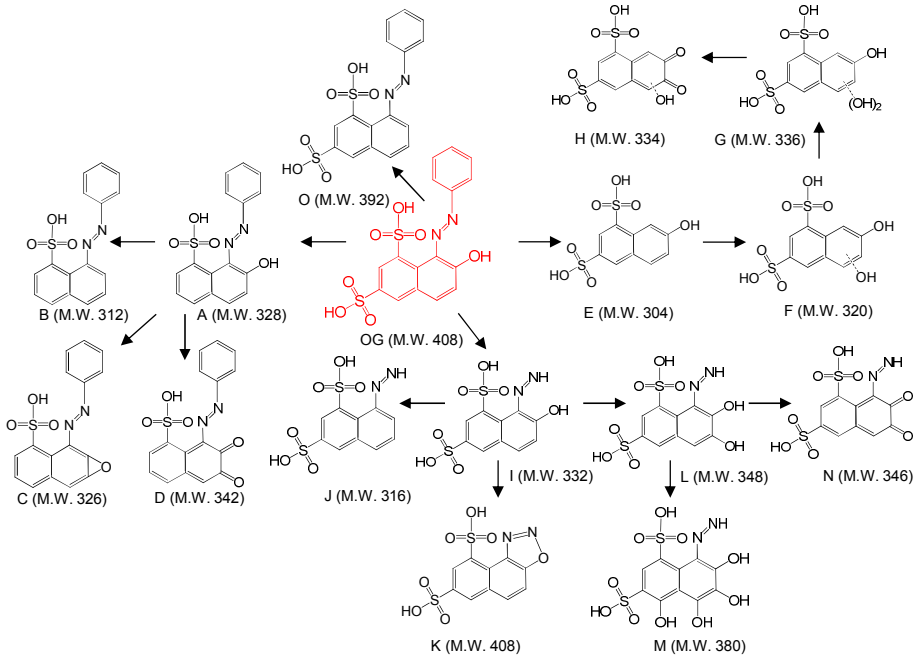

Fig. 6 Proposed mechanistic pathways of orange G degradation. All the products postulated are based on the analysis of LC-MS data.

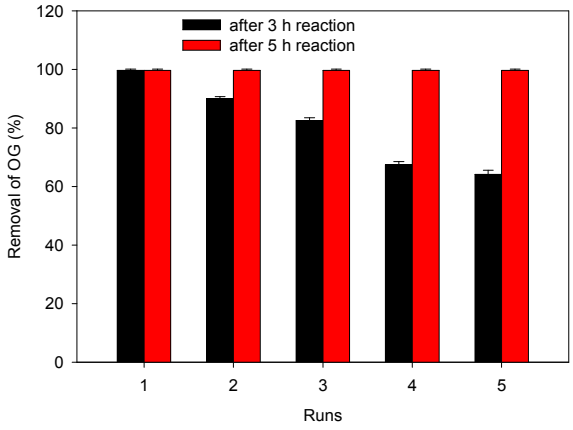

Fig. 7 Stability of nano-Co_3O_4 in consecutive runs. (Reaction conditions: $[OG]_0$=0.1 mM, $[PS]_0$=2.0 mM, [nano-Co_3O_4]=0.5 g L^{-1}, pH=7.0, T=25 ^oC, reaction time=3 h or 5 h).

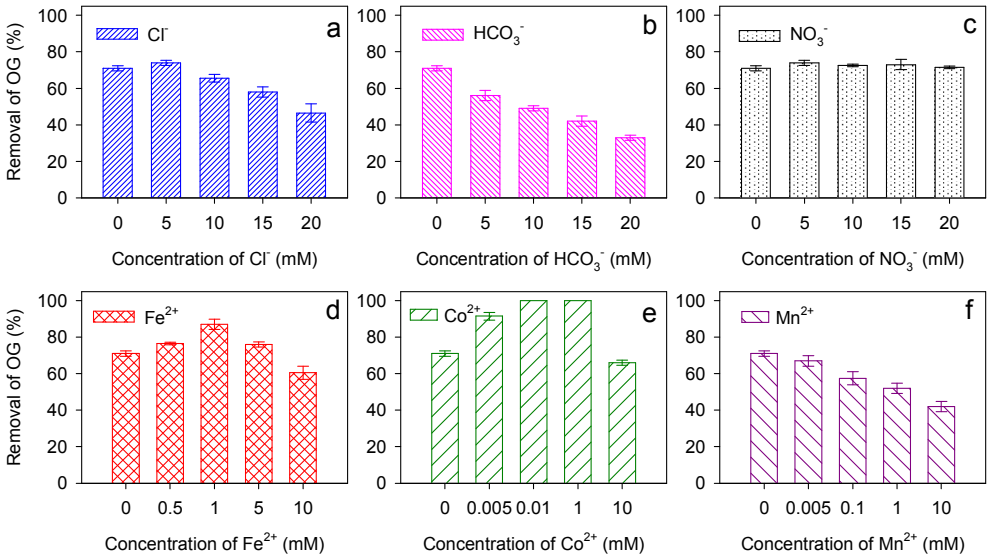

Fig. 8 Effects of co-existing water matrix chemicals on OG degradation in nano-Co_3O_4/PS process. (Reaction conditions: $[OG]_0$=0.1 mM, $[PS]_0$=2.0 mM, [nano-Co_3O_4]=0.5 g L^{-1}, pH=7.0, T=25 ^oC, reaction time=90 min).

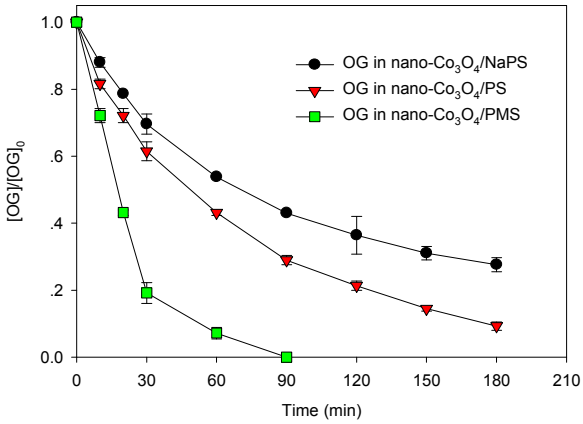

Fig. 9 OG degradation in nano-Co_3O_4/NaPS, nano-Co_3O_4/PS and nano-Co_3O_4/PMS processes. (Reaction conditions: [OG]=0.1 mM, [NaPS]=[PS]=[PMS]=2.0 mM, [nano-Co_3O_4]=0.5 g L^{-1}, pH=7.0±0.1, T=25 ^{o}C).